Chemical Engineering Science 157 (2017) 247–254

Contents lists available at ScienceDirect

Chemical Engineering Science

journal homepage: www.elsevier.com/locate/ces

Efficient separation of small microparticles at high flowrates using spiral channels: Application to waterborne pathogens

Melanie Jimenez [a,*], Brian Miller [b], Helen L. Bridle [a]

[a] IB3, Heriot-Watt University, Riccarton Edinburgh Campus, United Kingdom
[b] King's Building, University of Edinburgh, United Kingdom

HIGHLIGHTS

- Spiral channels investigated for the first time for separating waterborne pathogens.
- Impacts of rigid particle concentration, size and velocity evaluated.
- Results compared to behaviour of viable and non-viable pathogenic *Cryptosporidium*.
- 100% separation efficiency observed for *Cryptosporidium* at 500 μL/min.

ARTICLE INFO

Article history:
Received 25 June 2015
Received in revised form
13 August 2015
Accepted 23 August 2015
Available online 16 September 2015

Keywords:
Spiral microchannel
Separation
Pathogens
Drinking water

ABSTRACT

Detecting waterborne pathogens is a challenging task because of their low concentration in water and their wide diversity. In order to ease this detection process, the potential of microfluidics is investigated in this paper. Spiral channels are designed for separating particles, in a single device and without any external forces or additional buffer, depending on their size at high flowrates. This paper focuses first on the impact of the channel length, flowrate, particle concentration and size on the separation efficiency of polystyrene beads of relevant sizes (4–7 μm). The system is then tested with viable and non-viable pathogens (*Cryptosporidium parvum*) with an average size around 4–5 μm.

1. Introduction

Access to safe drinking is 'a human right that is essential for the full enjoyment of life and all human rights' as recognized by the United Nations General Assembly resolution (A/RES/64/292-2010). However, despite the current available treatments, several outbreaks are reported each month across Europe. Between 2000 and 2007, 47,617 episodes of illness have been reported in Europe by the European Environment and Health Information System (2009) while the Drinking Water Inspectorate (2012) reported around 60 significant events caused by waterborne pathogens in England and Wales in 2012. *Cryptosporidium* is one well-known and highly resistant protozoa encountered in water systems (Bridle et al., 2012; Bridle, 2013), which has been detected in water despite the absence of the target microbiological parameters (*Escherichia coli*, or faecal/thermotolerant coliforms; total coliforms; enterococci, faecal streptococci; and *Clostridium perfringens*) designated by the European Union for monitoring the water quality (WHO, 2014). A specific standardized procedure (namely US EPA 1623) is thus required for detecting its potential presence relying on (i) a filtration allowing large volumes of water to be treated while retaining all the particles of the same size or bigger than *Cryptosporidium*, (ii) an elution step to remove *Cryptosporidium* from the filter while (iii) centrifugation and immunomagnetic-separation are used for concentrating and isolating captured *Cryptosporidium* from other particles for detection. Highly experienced staff are then required to perform the detection by (iv) fluorescent labelling and microscopy (Bridle et al., 2012). This procedure is long (several days) and non-automated, delaying detection and thus potentially increasing the number of people affected in case of an outbreak. This protozoa is only one of many waterborne pathogens and one could easily imagine how challenging detecting accurately all the potential harmful pathogens is. The development of new tools enhancing the separation of pathogens by kingdom (virus, bacteria and protozoa) after filtration is thus required to enable a more automated/rapid process. This is particularly important with the growing interest in molecular methods for detection, as optimal lysis methodologies vary between different pathogen kingdoms. Due to its appropriate scale, microfluidics represents an interesting

* Corresponding author. Tel.: +44 131 451 4748.
E-mail address: M.Jimenez@hw.ac.uk (M. Jimenez).

http://dx.doi.org/10.1016/j.ces.2015.08.042

approach for working with small biological material, including *Cryptosporidium* as recently reviewed (Bridle et al., 2012, 2014). Studies have proposed a direct miniaturization of the final stages of the current process for microfluidic filtration and immuno-magnetic-separation although clogging issues and the specificity to single pathogens are still limiting their practical use by water companies. Dielectrophoresis is another technique proposed in the literature for concentrating and separating *Cryptosporidium* but the working flowrates are usually small, while hundreds of millimetres need to be analysed after filtration. There is thus a need in developing intermediate stages to process the large volumes of water obtained after filtration for promoting the potential of these microfluidic-based detection techniques.

The purpose of this paper is to try to fill this gap by proposing an efficient sized-based separation of pathogens after filtration at high flowrates. There is indeed an interesting correlation between the size of pathogens and their kingdom. For instance protozoa such as *Cryptosporidium* can be characterized by an ellipsoidal shape of about 5 μm in diameter (one should note that the size of *Cryptosporidium* also depends on its specie. The 5 μm figure corresponds to *C. parvum* and *hominis*, which are common problematic human pathogenic species whereas *Cryptosporidium muris* can size up to ≈ 7 μm in diameter). Pathogenic bacteria (≈ 1–3 μm) and viruses (≈ 20–100 nm) are smaller. The shape of pathogens can also drastically differ from one kingdom/specie to another, this point will be discussed later in the paper. In the literature, two main microfluidic techniques have been proposed for size-based particle separation at high flowrates (*e.g.*, in the mL/min range): deterministic lateral displacement (DLD) and inertial focusing (IF). As recently reviewed (McGrath et al., 2014), DLD can perform efficient separation in complex biological media such as blood. Although this technique has been successfully scaled up for separating 'angry pathogens' with LEGO ® for outreach activities (Jimenez and Bridle, 2015), the presence of posts in the channel makes DLD devices prone to clogging and thus potentially not suitable for routine procedures. To overcome this limitation, inertial focusing using spiral channels is considered for the first time in the literature for waterborne pathogen separation. The first part of this paper focuses on the different mechanisms behind inertial focusing in straight and spiral channels. Impacts of the particle concentration, size, velocity and channel length on focusing behaviour are then investigated with rigid polystyrene beads. The system is finally tested with pathogens and its potential as an interesting alternative for water companies discussed.

2. Principle of inertial focusing

The purpose of this section is to understand how a spiral channel as depicted in Fig. 1 can separate particles without any external forces. To start with focussing in straight channels is discussed.

2.1. Principle in straight channels

Considerable effort has gone into understanding why particles randomly distributed at the inlet of a straight channel tend to focus at some specific equilibrium positions at the outlet. This phenomenon has been attributed to the equilibration of two main effects: (i) a shear induced lift directed towards the channel walls due to the parabolic profile of velocity and (ii) a wall induced lift directing particles towards the channel centreline when the particle approaches the wall. The balance of these forces causes particles to equilibrate at a specific distance from the wall (Di Carlo, 2009). In square or rectangular channels, a third mechanism is involved, pushing particles towards the middle of channel faces,

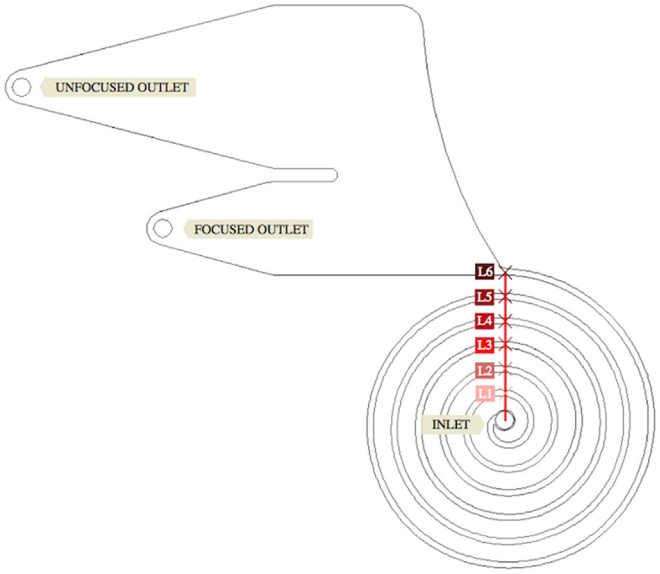

Fig. 1. The spiral microfluidic channel used for pathogens separation comprises 1 inlet in the centre of the spiral and 2 outlets. The depth of the device is 30 μm, the width 170 μm, and the pitch 500 μm.

and attributed to a rotation-induced lift (Zhou and Papautsky, 2013) or wall effects (Di Carlo, 2009; Amini et al., 2014). The net lift force F_L experienced by particles can be expressed as

$$F_L = C_L \times G^2 \times \rho \times a^4, \tag{1}$$

with C_L the lift coefficient, G the shear rate ($G = 2\overline{U}/D_h$, with $\overline{U}$ the average fluid velocity and D_h the channel hydraulic diameter), ρ the fluid density and a the particle diameter. Other formulations for this net lift force are proposed in the literature near the centreline ($\propto \rho \overline{U}^2 a^3/D$, D being the characteristic channel dimension) or the wall ($\propto \rho \overline{U}^2 a^6/D^4$) respectively. For further details, the interested reader is invited to consult the recent review of Amini et al. (2014).

As a consequence of these forces, particles tend to focus in the middle of the four faces in a square cross-section channel. In a rectangular cross-section channel, the velocity profile is sharper along the channel smallest dimension. The resulting shear lift is thus stronger along this direction leading to particles pushed towards the channels' longest faces. Similar to the behaviour in square channels, particles tend to focus in the middle of the channel faces resulting in two equilibrium positions in the middle of the longest faces.

2.2. Extension to spiral channels

In curved rectangular channels, the position of fluid maximum velocity shifts from the centre towards the concave wall of the channel due to a centrifugal action. In order to compensate this phenomenon, secondary rotating flows, namely Dean flows, appear in the channel (Nivedita et al., 2013). Particles flowing in a curved channel will thus experience a supplementary force, the Dean drag F_{DD}. Assuming the average Dean velocity proposed by Ookawara et al. (2004) ($\overline{U}_{DD} = 1.8 \times 10^{-4} De^{1.63}$), F_{DD} can be expressed as (Kuntaegowdanahalli et al., 2009)

$$F_{DD} = 5.4 \times 10^{-4} \mu De^{1.63} a, \tag{2}$$

μ being the fluid viscosity and De the Dean number defined as

$$De = \frac{\rho \overline{U} D_h}{\mu} \times \sqrt{\frac{D_h}{2R}}, \tag{3}$$

with R the radius channel curvature.

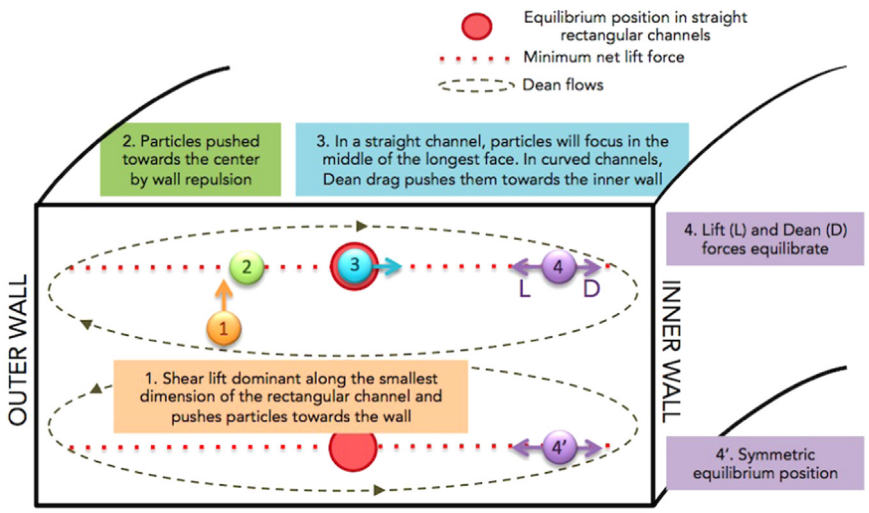

Fig. 2. Schematic illustrating the simplified mechanisms involved in focusing particles against the inner wall of a spiral channel.

Table 1
Literature research in terms of focusing of particles smaller than 5 μm in straight and curved channels using inertial focusing.

Authors	Min. size (μm)	Channel type	Height × width (μm)
Ciftlik et al. (2013)	2	Straight	10 × 16
Bhagat et al. (2008c)	1.9	Straight	20 × 50
Masaeli et al. (2012)	3	Straight	47 × [25, 30, 35]
Russom et al. (2009)	≈ 5	Curved	50 × [250–1090]
Gossett and Di Carlo (2009)	2.2	Curved	20 μm in width
Xiang et al. (2013b)	4.8	Curved	50 × 160

It can be noted that both the net lift force and the Dean drag are a function of the fluid velocity and consequently strongly depend on the applied flowrate. Assuming an appropriate flowrate, the equilibrium of the net lift force presented above and the Dean drag leads to new equilibrium positions near the convex (inner) wall of the channel. Guan et al. (2013) have recently proposed an interesting analysis of this mechanism that will briefly be summarized here. In curved channels, particles first experience the net lift force and tend to go to minimum lift force planes. Once particles are positioned in planes, the Dean drag acts and pushes particles towards the inner wall (*cf.* Fig. 2).

Since all the forces involved here are a function of the size of particles ($F_L/F_{DD} \propto a^3$), the equilibrium positions of particles depend on their size. This technique has been successfully applied for separating beads (Bhagat et al., 2008a,b; Guan et al., 2013; Lee et al., 2011; Kuntaegowdanahalli et al., 2009; Russom et al., 2009; Nivedita et al., 2013; Xiang et al., 2013a) or biological components such as cancer cells, red blood cells or white blood cells (Di Carlo et al., 2007; Goda et al., 2012; Ozkumur et al., 2013; Tanaka et al., 2012; Nivedita et al., 2013). However the number of papers targeting the focussing of particles smaller than 5 μm remains low (Table 1). Additionally, these studies focused their work on rigid spherical beads. This paper aims to deepen the comprehension of focusing behaviours of small model particles and explore how this theory extends to the separation of small biological material (*e.g.*, pathogens).

3. Materials and methods

3.1. Microfluidic system

Experimental results presented in this paper are obtained with the spiral channel presented in Fig. 1. The focussing channel consists of 6 loops, is 30 μm in depth and 170 μm in width. The device has one inlet (in the middle of the spiral) and two outlets for collecting particles. Pathogens present a wide range of sizes and shapes allowing them to focus at different locations in the channel. By proposing a 2-outlet system, pathogens are more likely to be separated in the same outlet. It was also observed that although the spiral itself remained clean after numerous tests, if particles remained in the device they did so right after the openings where the velocity profile is lower. By proposing 2 outlets only, the system is less sensitive to the presence of blocked particles near the outlets, which could strongly alter the trajectory of focused particles and hinder an effective separation. The outlets are much wider than the main channel to better discriminate focusing positions. The device has been manufactured by lithography with a combination of Epoxy and PMMA (Epigem, UK). The inlet is connected to a syringe-pump (Harvard-Apparatus, US) *via* 1/16 in PTFE tubing of 0.5 mm internal diameter (Thames Restek, UK). The radius of curvature in the channel varies between 0.65 mm (first loop *L*1) and 3.95 mm (6th loop *L*6). This device is supposed to focus particles larger than 2.1 μm based on the criterion $a/H > 0.07$ (Kuntaegowdanahalli et al., 2009) or 3.0 μm if $a/H > 0.1$ (Russom et al., 2009), a being the particle diameter and H the smallest dimension of the rectangular channel cross-section. The ratio of shear gradient lift and Dean drag as proposed by Russom et al. (2009), $R_f = 2a^2R/H^3$ (R being the radius of curvature) also easily satisfies the condition $R_f > 0.08$ for particles considered here (Amini et al., 2014). Flowrates range from 100 to 500 μL/min corresponding to channel Reynolds numbers between 25 and 125.

3.2. Characteristics of particles

As presented in Table 2, different polystyrene beads (PS) have been used to calibrate the system and establish the equilibrium positions for different sized entities. The beads size range is in accordance with characteristic sizes of different *Cryptosporidium* species (Bridle, 2013).

Subsequently tests have been performed with viable and non-viable (killed by heat treatment) *C. parvum* (Waterborne Inc, US) in deionized water. It can be noted here that the cost of a few millilitres of pathogens at a concentration of around 1×10^6 cells/mL easily exceeds hundreds of dollars and in addition requires class 2 safety laboratories to be handled. There is thus a real interest in comparing the behaviour of beads and pathogens to find a relevant and less expensive surrogate.

3.3. Measurement systems

Single particles (beads and pathogens) have been imaged in the microfluidic device with a fluorescent inverted microscope (Nikon, $\times 10$ or $\times 25$ magnification) and a high speed camera (CCD ProgRes ®, Jenoptik, Germany). The impact of the concentration of beads has been evaluated with a microscope camera (Dino-Lite Digital Microscope, Taiwan).

In order to quantify separation efficiencies, particle size distributions at the inlet and both outlets have been measured using a Malvern MasterSizer S (the Malvern MasterSizer S is a single lens laser diffraction system, using a small helium neon laser of the order of 2 mW power to measure the size of particles). It can be noted that distributions provided by this equipment are functions of the particle volume. The presence of large objects such as bubbles can thus decrease the probability of detecting smaller particles.

Results obtained with the MasterSizer have been compared with a direct observation of beads on a membrane. Microliters of the collected samples in both outlets were passed through a 0.22 μm pore size membrane (MF-Millipore membranes) with retained beads counted using a microscope. Results obtained using this direct observation validated the results from the MasterSizer. In the following sections, only the MaterSizer data are presented.

The efficiency of the system for separating *C. parvum* has been evaluated by experienced staff at Scottish Water by counting the number of pathogens in the outlets *via* fluorescent labelling with antibodies.

Table 2
Characteristics of polystyrene beads used. The size is the average diameter of beads and SD is the standard deviation provided by the manufacturer.

Average particle size	Property	Manufacturer
7.50 μm ($SD = 0.09$ μm)	Coloured Red	microparticles GmbH, Germany
5.21 μm ($SD = 0.08$ μm)	Coloured Blue	microparticles GmbH, Germany
5.00	Green fluorescent	Micromods, Germany
4.00	Green fluorescent	Micromods, Germany

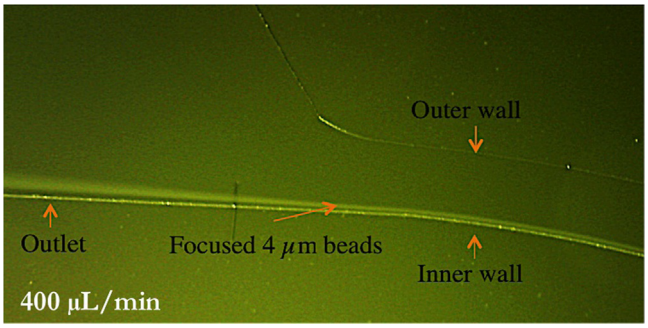

Fig. 3. Visualization of the behaviour of 4.0 μm PS beads at the outlet of the spiral channel at 400 μL/min. The flow is directed from the right towards the left of the figure.

4. Results

4.1. Qualitative imaging

The first tests were performed with beads and the microscope camera (Dino-Lite) near the outlet of the system (*L*6 in Fig. 1). Results obtained with 4.0 and 7.5 μm PS beads are presented in Figs. 3 and 4. Fig. 3 indicates that at 400 μL/min 4 μm PS beads are tightly focused against the inner wall of the channel due to balance of the forces schematically presented in Fig. 2.

The left hand side plot of Fig. 4 depicts a flow of non-focused particles when the flowrate is too low (< 50 μL/min), conversely to the right hand side plot associated with a higher flowrate (400 μL/min). As expected, higher flowrates result in a focusing effect near the inner wall which is the ideal scenario for water applications due to the associated large volumes.

For a similar flowrate (400 μL/min), larger particles (7.5 μm) appear to be closer to the centreline than 4.0 μm PS beads. This result is however counter-intuitive: if particles are pushed against the wall due to the Dean forces ($F_{DD} \propto a$), larger particles should be closer to the wall as reported in other studies (Russom et al., 2009; Kuntaegowdanahalli et al., 2009; Lee et al., 2011; Nivedita et al., 2013). However, and as visible in Fig. 4 (right), beads in this experiment appear to be less tightly focused after the channel opening than the 4.0 μm PS beads (Fig. 3). This phenomenon is actually due to strong particle–particle interactions at high particle concentration. Fig. 5(a) and (b) presents the behaviour of 7.5 μm beads in similar conditions as in Fig. 4 (right) at the very beginning of the microchannel, *i.e.*, at the first (*L*1) and second (*L*2) loop of the spiral. Three streams are observed instead of one as expected in a rectangular channel from a top view. This phenomenon has already been reported in straight channels at high volume fraction ϕ (Humphry et al., 2010). In their work, Humphry et al. (2010) observed three streams of 9.9 μm beads in 160×25 μm^2 straight rectangular channels when $\phi > 0.015$ due to steric interactions between particles. This phenomenon is also observed here in spiral channels in conditions where $\lambda = 6WH\phi/\pi a^2 > 1$ in

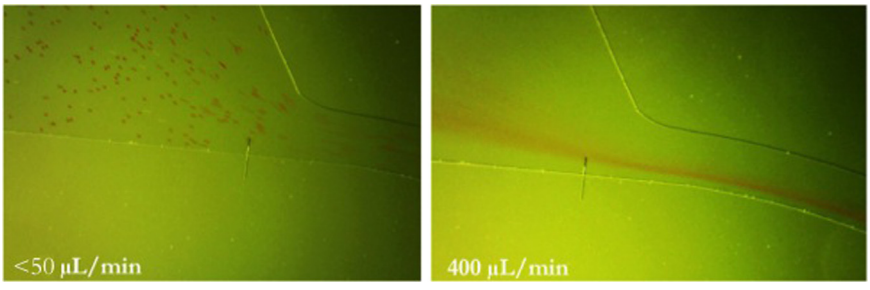

Fig. 4. Visualization of the behaviour of 7.5 μm PS beads at the outlet of the spiral channel at 50 μL/min (left) and 400 μL/min (right). The flow is directed from the right towards the left of the figure.

accordance with Di Carlo (2009). Due to the Dean forces acting towards the inner wall, these streams tend to merge near the inner wall loop after loop, although the channel length seems to be insufficient to perfectly focus beads into a narrow stream at the outlet for this flowrate (400 μL/min). When the bead concentration is decreased to 1.1×10^7 particles/mL (corresponding to $\phi = 0.002$) a single tight stream is observed as depicted in Fig. 5(d).

To avoid the presence of multiple streams that are hindering the separating process, tests have been carried out at lower volume fractions. A mixture of 7.5 μm (red) and 5.2 μm (blue) PS beads has been introduced to determine whether or not larger particles remain closer to the centreline at 400 μL/min as mentioned previously. For a better visualization, images have been recorded just after stopping the inlet flow as depicted in Fig. 5(c). It clearly appears here that the smallest beads (blue beads) are closer to the inner wall. A similar trend has been observed at low flowrates (< 1 mL/min) in the recent work of Guan et al. (2013) for 5.8, 9.8, 15.5 and 26.3 μm beads. For higher flowrates ($\approx < 4$ mL/min), they observed a shift of larger particles closer to the inner wall as one would expect. This phenomenon could be attributed to a wall induced lift (scaling as $F_W \propto a^3/\delta$; Stephen Williams et al., 1994) which is strong enough at lower flowrates for pushing the largest particles further from the inner wall. It has been observed in the literature that an increase in the flowrate usually tends to push particles closer to the walls due to the shear induced lift dominating over the wall induced lift (Di Carlo et al., 2007; Amini et al., 2014). It is reasonable to think that in this range of flowrates (≈ 400 μL/min here), particles start to focus but the wall induced lift keeps the largest ones towards the centreline. This effect would disappear when increasing the flowrate. Table 3 presents the average location of 7.5 μm beads in the spiral near the oultlets (*L*6 in Fig. 1). A mean position at 0 μm (resp. 170 μm) means that particles are on average against the outer (resp. inner) wall. It clearly appears in this table that the larger the flowrate, the closer the 7.5 μm beads to the inner wall.

4.2. Determination of separation efficiencies

It has been demonstrated previously that the particle concentration strongly alters the focusing behaviour. Although only one stream has been detected for a concentration of 1.1×10^7 particles/mL, proving that 7.5 μm beads are narrowly focused and separated remains challenging based on the quality of images depicted in the previous section. In order to quantify the separation efficiency, particle size distributions are measured at the outlets of the system with a Malvern MasterSizer S. As mentioned previously, since particle size distributions are depicted in volume of the presence of large objects such as bubbles can decrease the probability to detect smaller particles in the sample. Each test has been performed with a constant flowrate of 400 μL/min and with 7.5 μm PS beads only.

For concentrations below 2.6×10^6 particles/mL, no particles are detected in the size range of beads in the unfocused outlet (outlet corresponding to the 'waste', with particles that are not focused). However as presented in Fig. 6, above this concentration the focussing is less effective resulting in the presence of particles in the unfocused outlet. It appears in Fig. 7, corresponding to a sample with water and surfactant only, that the particles larger than 100 μm visible in Fig. 6 (bottom panel) are actually bubbles or undissolved surfactant.

4.3. Quantitative imaging

4.3.1. Focussing of PS beads

In order to go deeper into the understanding of particle behaviour in spiral channels, single particles (beads and pathogens) have been imaged with a high-speed camera at different lengthwise positions and flowrates inside the channel. Concentrations and number of particles detected for these experiments are presented in Table 4.

Representative results obtained with 4 μm beads are presented in Fig. 8. This graph plots the distribution of particles as a function of the distance to the outer wall (the channel width being 170 μm) near the outlet (*L*6 in Fig. 1) and at different flowrates (between 200 and 400 μL/min, *i.e.*, channel Reynolds numbers between 50 and 125). Each distribution has been normalized by its area below the curve to take into account the difference number of detected particles for each test. Fig. 8 shows that a narrow peak is detected near the inner wall when the flowrate increases. At lower flowrates (*e.g.*, 200 μL/min), some particles are not totally focused and remain closer to the centreline. A flowrate of 400 μL/min is required here to tightly focus 4 μm beads. Similar experiments

Table 3
Mean position of 7.5 μm beads near the outlets of the spiral (*L*6 in Fig. 1) at different flowrates. Mean positions represent the average location of imaged beads in the channel with 0 μm (resp. 170 μm) being the outer (resp. inner) wall of the channel.

Flowrate (μL/min)	Mean position (μm)
400	128.0
500	132.9
700	141.4
900	147.3
1100	154.6
1500	165.5

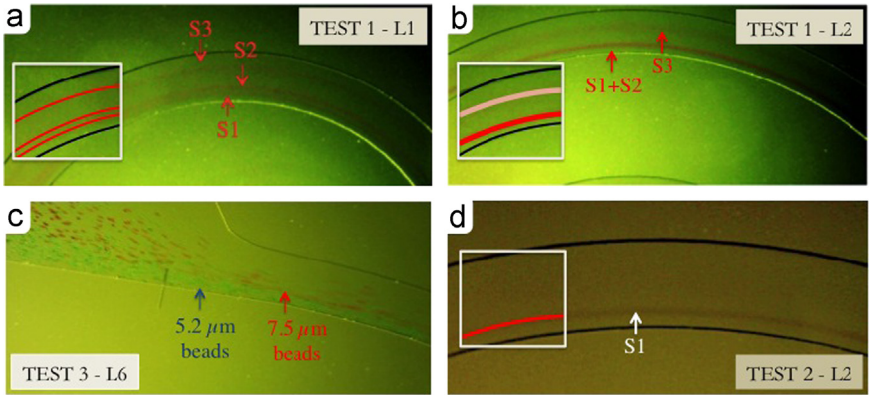

Fig. 5. Visualization of the behaviour of 7.5 μm PS beads at the first (a) and second loop of the spiral channel at 400 μL/min at high (b) and low (d) volume fractions. Visualization of the focusing positions of 7.5 μm (red) and 5.2 μm (blue) PS beads just after stopping the inlet flow. Inserts represent a magnified view of these streaks with colours exaggerated for a better visualization. (For interpretation of the references to colour in this figure caption, the reader is referred to the web version of this paper.)

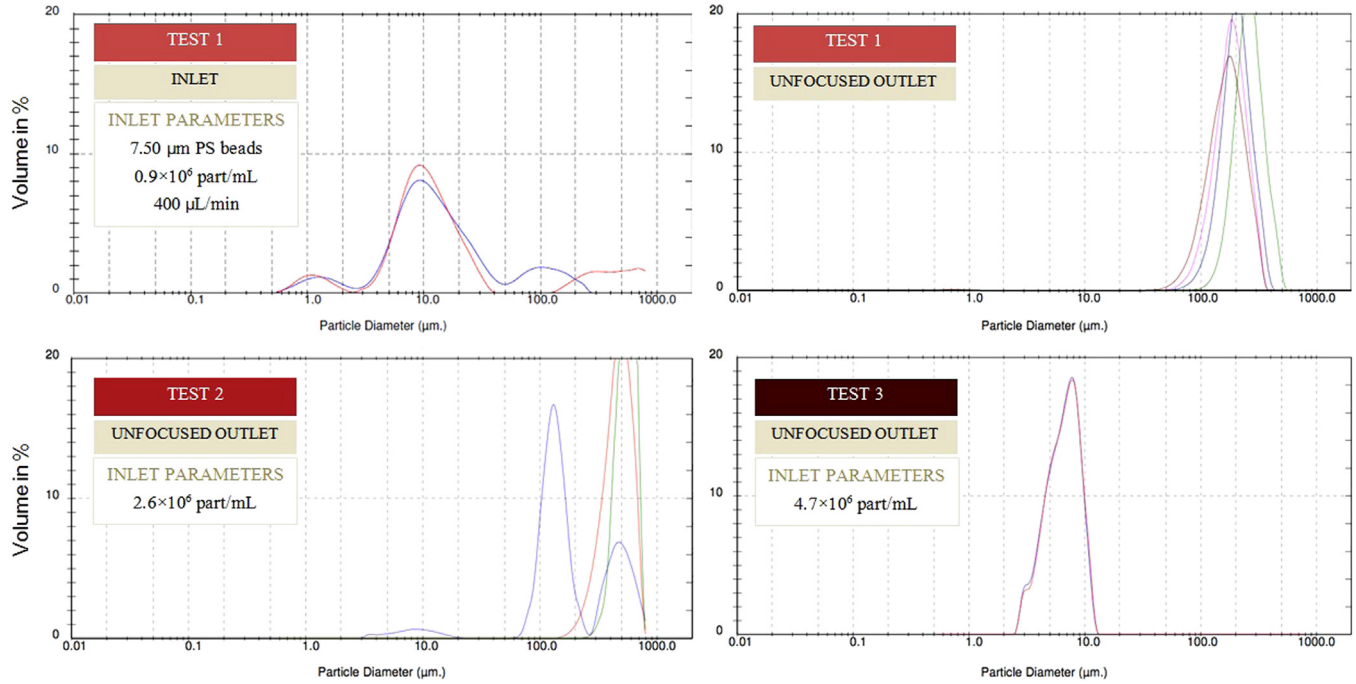

Fig. 6. Size distribution in volume of 7.5 μm PS beads at the inlet (top-left) and unfocused outlets with an initial concentration in beads of 0.9×10^6 particles/mL (top-right), 2.6×10^6 particles/mL (bottom-left) and 4.7×10^6 particles/mL (bottom-right).

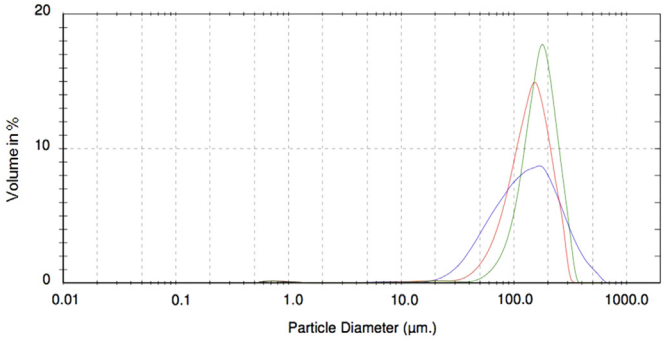

Fig. 7. Size distribution in DI water and a small amount of surfactant (Triton X).

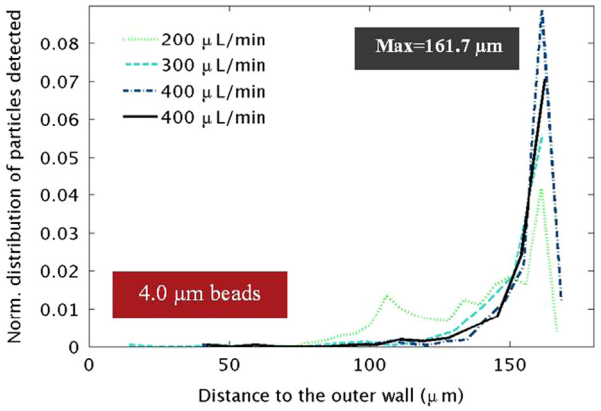

Fig. 8. Normalized distribution of the position of 4 μm particles as a function of the distance to the outer wall and for different flowrates. Distributions are estimated by imaging the position of single particles near the outlet of the channel with a high-speed camera. The main mode of these distributions is at about 8 μm from the inner wall. The channel inner wall is at 170 μm.

Table 4
Characteristics (size and concentration) of polystyrene beads used and average number of beads detected for each experiment using the high-speed camera.

Particle size (μm)	Concentration (part/mL)	Number of part. detected
7.50	0.9×10^6	121
5.21	2.6×10^6	429
5.00	3.6×10^6	301
4.00	35×10^6	420

have been carried out with particles presenting a larger diameter. Results are summarized in Fig. 9 with markers corresponding to the main modes of the distributions for different particle sizes and flowrates or channel Reynolds numbers (the mode corresponds to the most probable position of particles for a given condition, *e.g.*, 161.7 μm for 4 μm beads at 400 μL/min in Fig. 8). Lines below the markers represent the standard deviation of the distribution defined as $\left(1/(n-1)\sum_{i=1}^{n}(x_i-\overline{x})^2\right)^{0.5}$, n being the number of elements in the sample and $\overline{x}$ the mean value. It clearly appears that larger particles remain closer to the centreline as previously stated and that higher flowrates decrease the standard deviation as a result of a narrower focussing stream. Particles tend also to be closer to the inner wall when increasing the flowrate due to a stronger Dean force ($\propto \overline{U}^{1.63}$).

Similar experiments have been performed at 400 μL/min and different locations in the spiral (*cf.* definition of loop numbers in Fig. 1). The evolution of the standard deviation of the particle position within the channel cross-section is plotted loop after loop in Fig. 10 for different particle sizes. It can be noted here that lines between markers have only been added in the graph to help the reader see the trend when increasing the number of loop for a given particle size. As expected the standard deviation decreases when increasing the number of loop. For larger particles, the standard deviation remains almost constant after the 5th loop.

4.3.2. *Focussing of pathogens*

For the last experiment, human pathogenic *C. parvum* have been diluted in deionized water, without surfactant, and passed through the spiral channel. This pathogen presents a slightly ellipsoidal shape

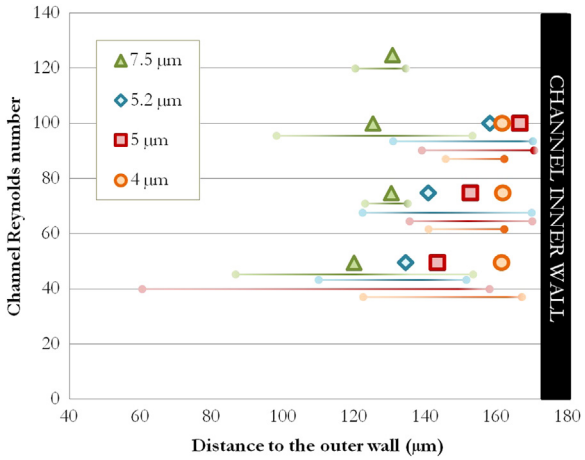

Fig. 9. Position of the main mode (marker) and standard deviation (line) of different particles near the outlet as a function of the channel Reynolds number. For clarity and to avoid overlapping of data markers the standard deviations are represented below the markers by decreasing particle size.

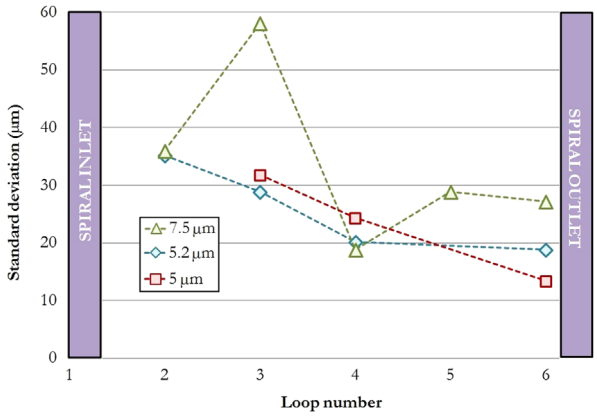

Fig. 10. Evolution of the standard deviation loop after loop of the position of particles flowing at 400 μL/min. Definition of loop numbers is in Fig. 1.

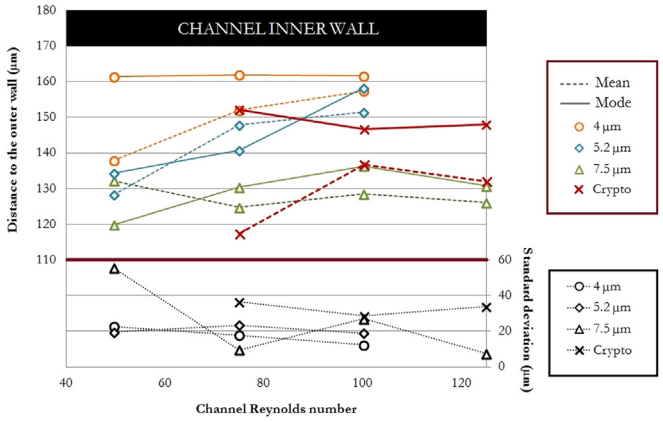

Fig. 11. Evolution of the standard deviation loop after loop of the position of PS beads and *Cryptosporidium parvum* flowing at 400 μL/min. Definition of loop numbers is in Fig. 1.

and an average size around 5 μm ($\approx 4.5 \times 5.5\ \mu m^2$). The behaviour of this pathogen is also imaged with the high speed camera and characterized by analysing its distribution as a function of distances to the outer wall as presented previously. The behaviour of *C. parvum* is compared to results reported with PS beads in Fig. 11. On the top part of this figure, mean and main mode of the particle position distribution are compared for different channel Reynolds numbers. The standard deviation is plotted in the bottom part of the graph. It appears that *C. parvum* behaves mostly like 5.2 μm particles, which are the closest match in terms of size. Mean values of *Cryptosporidium* positions are however closer to the behaviour of 7.5 μm beads possibly because of the presence of larger *Cryptosporidium* in the sample (or another larger contaminant) or due to their deformability. For channel Reynolds number larger than 100, the mean, mode and standard deviation for *Cryptosporidium* remain the same.

It could be expected that pathogens focus at equilibrium positions closer to the centreline than rigid beads of an identical size as observed in the literature for other biological cells. Both the cell shape and deformability can alter its behaviour in the channel. It has been observed for instance in straight channels that ellipsoidal particles followed a tumbling motion causing a higher wall lift force when the major axis is perpendicular to the wall. As a consequence, the equilibrium positions of symmetric particles are closer to the centreline but are the same as for a sphere of similar rotational diameter (Amini et al., 2014; Hur et al., 2011a; Masaeli et al., 2012). If the particle is deformable, an additional centre-directed lift is induced pushing the equilibrium positions also usually closer to the centreline (Amini et al., 2014; Hur et al., 2011b).

Since some *C. parvum* present a similar behaviour to 7.5 μm PS beads and that it has been presented previously that depending on their concentration, some particles of this size can be deviated in the wrong outlet (*i.e.*, unfocused outlet in Fig. 1) the separation efficiency of this pathogen is evaluated. To avoid any contamination of the Malvern MasterSizer S with live harmful pathogens, experienced staff from Scottish Water counted by fluorescent labelling with antibodies the number of pathogens in both outlets. For that purpose, roughly 3 mL of samples at both outlets were filtered on a small membrane and then fluorescently labelled. The number of pathogens was counted on the membrane by using a fluorescent microscope. It has been reported that 100% of *C. parvum* were in the focused outlet for a given flowrate of 400 μL/min. No major difference has been noted between viable and non-viable pathogens. It should be mentioned here that despite this excellent separation efficiency, the recovery rate was not 100%. Due to the large openings at the end of the spiral, particles decelerate and tend to stick to the walls of the channel. The spiral itself remains clear after several uses but particles tend to aggregate at the outlets. Although not critical for the separation itself, the recovery rate is impacted. Efforts are currently focused on (i) quantifying this loss and (ii) minimizing it.

5. Conclusions

Inertial focusing in spiral channels was investigated for the first time for separating and concentrating waterborne pathogens such *Cryptosporidium*. Rigid polystyrene beads, of similar sizes to pathogens, from 4 to 7.5 μm have been successfully focused with channel Reynolds numbers of about 100. The impact of the concentration has been evaluated with the presence of multiple streams at high volume fraction observed. The impact of the flowrate and channel length has also been investigated by imaging single particles with a high speed camera. Depending on their sizes, beads focused at different equilibrium positions allowing a size-based separation. Interestingly, in the range of flowrates considered in this study, larger PS beads presented equilibrium positions closer to the channel centreline. Based on these promising results, the technique has been used with viable and non-viable pathogens which have been observed to experience also the focusing effect. *C. parvum* are found to focus slightly closer to the channel centreline in comparison with spheres of similar size. This phenomenon can be attributed to the pathogen deformability or a non-homogeneity in pathogen sizes. Other techniques allowing the measurement of

pathogen size distribution and concentration are under investigation to further characterize the efficiency of this technique for pathogen separation. The technique will then be extended to other protozoa with a more complex shape such as *Giardia lamblia* presenting a more flattened aspect than *Cryptosporidium*.

Acknowledgements

H.B. and M.J. would like to acknowledge EU funding for the project 'AQUAVALENS: protecting the health of Europeans by improving methods for the detection of pathogens in drinking water and water used in food preparation'. H.B. would like to acknowledge The Royal Academy of Engineering/EPSRC for her research fellowship. B.M. would like to acknowledge his BBSRC Industrial Case Studentship, supported by Scottish Water. M.J., B.M. and H.B. would like to acknowledge Epigem for the manufacturing part, Scottish Water for pathogens counting, and Deonie Allen (HWU) for her help with size distribution measurements.

References

Amini, Hamed, Lee, Wonhee, Di Carlo, Dino, 2014. Inertial microfluidic physics. Lab Chip 14, 2739–2761.

Bhagat, Ali Asgar S., Kuntaegowdanahalli, Sathyakumar S., Dionysiou, Dionysios D., Papautsky, Ian, 2008a. Spiral microfluidic nanoparticle separators. In: MOEMS-MEMS 2008 Micro and Nanofabrication. International Society for Optics and Photonics, pp. 68860M–68860M.

Bhagat, Alia Asgar S., Kuntaegowdanahalli, Sathyakumar S., Papautsky, Ian, 2008b. Continuous particle separation in spiral microchannels using dean flows and differential migration. Lab Chip 8, 1906–1914.

Bhagat, Ali Asgar S., Kuntaegowdanahalli, Sathyakumar S., Papautsky, Ian, 2008c. Enhanced particle filtration in straight microchannels using shear-modulated inertial migration. Phys. Fluids 20 (10), 101702.

Bridle, Helen, 2013. Waterborne Pathogens: Detection Methods and Applications. Newnes.

Bridle, Helen, Kersaudy-Kerhoas, Maïwenn, Miller, Brian, Gavriilidou, Despoina, Katzer, Frank, Innes, Elisabeth A., Desmulliez, Marc P.Y., 2012. Detection of cryptosporidium in miniaturised fluidic devices. Water Res. 46 (6), 1641–1661.

Bridle, Helen, Miller, Brian, Desmulliez, Marc P.Y., 2014. Application of microfluidics in waterborne pathogen monitoring: a review. Water Res. 55, 256–271.

Ciftlik, Ata Tuna, Ettori, Maxime, Gijs, Martin A.M., 2013. High throughput-per-footprint inertial focusing. Small 9 (16), 2764–2773.

Di Carlo, Dino, 2009. Inertial microfluidics. Lab Chip 9, 3038–3046.

Di Carlo, Dino, Irimia, Daniel, Tompkins, Ronald G., Toner, Mehmet, 2007. Continuous inertial focusing, ordering, and separation of particles in microchannels. Proc. Natl. Acad. Sci. 104 (48), 18892–18897.

Drinking Water Inspectorate, 2012. Drinking Water 2012.

European Environment and Health Information System, 2009. Outbreaks of Waterborne Diseases. Fact Sheet 1.1.

Goda, Keisuke, Ayazi, Ali, Gossett, Daniel R., Sadasivam, Jagannath, Lonappan, Cejo K., Sollier, Elodie, Fard, Ali M., Claire Hur, Soojung, Adam, Jost, Murray, Coleman, et al., 2012. High-throughput single-microparticle imaging flow analyzer. Proc. Natl. Acad. Sci. 109 (29), 11630–11635.

Gossett, Daniel R., Di Carlo, Dino, 2009. Particle focusing mechanisms in curving confined flows. Anal. Chem. 81 (20), 8459–8465.

Guan, G., Wu, L., Bhagat, A.A., et al., 2013. Spiral microchannel with rectangular and trapezoidal cross-sections for size based particle separation. Sci. Rep. 3, 1475.

Humphry, Katherine J., Kulkarni, Pandurang M., Weitz, David A., Morris, Jeffrey F., Stone, Howard A., 2010. Axial and lateral particle ordering in finite Reynolds number channel flows. Phys. Fluids 22 (8), 081703.

Hur, Soojung Claire, Choi, Sung-Eun, Kwon, Sunghoon, Di Carlo, Dino, 2011a. Inertial focusing of non-spherical microparticles. Appl. Phys. Lett. 99 (4), 044101.

Hur, Soojung C., Henderson-MacLennan, Nicole K., McCabe, Edward R.B., Di Carlo, Dino, 2011b. Deformability-based cell classification and enrichment using inertial microfluidics. Lab Chip 11, 912–920.

Jimenez, Melanie, Bridle, Helen L., 2015. Angry pathogens, how to get rid of them: introducing microfluidics for waterborne pathogen separation to children. Lab Chip 15, 947–957.

Kuntaegowdanahalli, Sathyakumar S., Bhagat, Ali Asgar S., Kumar, Girish, Papautsky, Ian, 2009. Inertial microfluidics for continuous particle separation in spiral microchannels. Lab Chip 9 (20), 2973–2980.

Lee, Wong Cheng, Bhagat, Ali Asgar S., Huang, Sha, van Vliet, Krystyn J., Han, Jongyoon, Lim, Chwee Teck, 2011. High-throughput cell cycle synchronization using inertial forces in spiral microchannels. Lab Chip 11 (7), 1359–1367.

Masaeli, Mahdokht, Sollier, Elodie, Amini, Hamed, Mao, Wenbin, Camacho, Kathryn, Doshi, Nishit, Mitragotri, Samir, Alexeev, Alexander, Di Carlo, Dino, 2012. Continuous inertial focusing and separation of particles by shape. Phys. Rev. X 2 (3), 031017.

McGrath, J., Jimenez, M., Bridle, H., 2014. Deterministic lateral displacement for particle separation: a review. Lab Chip 14 (21), 4139–4158.

Nivedita, N., Ligrani, P., Papautsky, I., 2013. Evolution of secondary dean vortices in spiral microchannels for cell separations. In: 17th International Conference on Miniaturized Systems for Chemistry and Life Sciences, Freiburg, Germany.

Ookawara, Shinichi, Higashi, Ryochi, Street, David, Ogawa, Kohei, 2004. Feasibility study on concentration of slurry and classification of contained particles by microchannel. Chem. Eng. J. 101 (1), 171–178.

Ozkumur, Emre, Shah, Ajay M., Ciciliano, Jordan C., Emmink, Benjamin L., Miyamoto, David T., Brachtel, Elena, Yu, Min, Chen, Pin-i, Morgan, Bailey, Trautwein, Julie, et al., 2013. Inertial focusing for tumor antigen-dependent and-independent sorting of rare circulating tumor cells. Sci. Transl. Med. 5 (179) (179ra47–179ra47).

Russom, Aman, Gupta, Amit K., Nagrath, Sunitha, Di Carlo, Dino, Edd, Jon F., Toner, Mehmet, 2009. Differential inertial focusing of particles in curved low-aspect-ratio microchannels. N. J. Phys. 11 (7), 075025.

Stephen Williams, P., Lee, Seungho, Calvin Giddings, J., 1994. Characterization of hydrodynamic lift forces by field-flow fractionation. Inertial and near-wall lift forces. Chem. Eng. Commun. 130 (1), 143–166.

Tanaka, Tatsuya, Ishikawa, Takuji, Numayama-Tsuruta, Keiko, Imai, Yohsuke, Ueno, Hironori, Matsuki, Noriaki, Yamaguchi, Takami, 2012. Separation of cancer cells from a red blood cell suspension using inertial force. Lab Chip 12 (21), 4336–4343.

WHO, 2014. Report on Regulations and Standards for Drinking Water Quality.

Xiang, Nan, Chen, Ke, Sun, Dongke, Wang, Shanfang, Yi, Hong, Ni, Zhonghua, 2013a. Quantitative characterization of the focusing process and dynamic behavior of differently sized microparticles in a spiral microchannel. Microfluid. Nanofluid. 14 (12), 89–99.

Xiang, Nan, Yi, Hong, Chen, Ke, Sun, Dongke, Jiang, Di, Dai, Qing, Ni, Zhonghua, 2013b. High-throughput inertial particle focusing in a curved microchannel: insights into the flow-rate regulation mechanism and process model. Biomicrofluidics 7 (4).

Zhou, Jian, Papautsky, Ian, 2013. Fundamentals of inertial focusing in microchannels. Lab Chip 13, 1121–1132.